Since January 2020 Elsevier has created a COVID-19 resource centre with free information in English and Mandarin on the novel coronavirus COVID-19. The COVID-19 resource centre is hosted on Elsevier Connect, the company's public news and information website.

International Journal of Biological Macromolecules 221 (2022) 71–82

Contents lists available at ScienceDirect

International Journal of Biological Macromolecules

journal homepage: www.elsevier.com/locate/ijbiomac

Unfolding of the SARS-CoV-2 spike protein through infrared and ultraviolet-C radiation based disinfection

Nilkamal Mahanta [a], Swati Sharma [b], Laipubam Gayatri Sharma [b], Lalit M. Pandey [b], Uday Shanker Dixit [a,*]

[a] Department of Mechanical Engineering, Indian Institute of Technology Guwahati, India
[b] Bio-Interface and Environmental Engineering Laboratory, Department of Biosciences and Bioengineering, Indian Institute of Technology Guwahati, India

ARTICLE INFO

Keywords:
Disinfection box
Infrared irradiation
Broad-spectrum antibacterial activity
Spike protein
Unfolding of proteins
Inactivation of coronavirus

ABSTRACT

The spreading of coronavirus from contacting surfaces and aerosols created a pandemic around the world. To prevent the transmission of SARS-CoV-2 virus and other contagious microbes, disinfection of contacting surfaces is necessary. In this study, a disinfection box equipped with infrared (IR) radiation heating and ultraviolet-C (UV-C) radiation is designed and tested for its disinfection ability against pathogenic bacteria and SARS-CoV-2 spike protein. The killing of a Gram-positive, namely, *S. aureus* and a Gram-negative namely, *S. typhi* bacteria was studied followed by the inactivation of the spike protein. The experimental parameters were optimized using a statistical tool. For the broad-spectrum antibacterial activity, the optimum condition was holding at 65.61 °C for 13.54 min. The killing of the bacterial pathogen occurred via rupturing the cell walls as depicted by electron microscopy. Further, the unfolding of SARS-CoV-2 spike protein and RNase A was studied under IR and UV-C irradiations at the aforesaid optimized condition. The unfolding of both the proteins was confirmed by changes in the secondary structure, particularly an increase in β-sheets and a decrease in α-helixes. Remarkably, the higher penetration depth of IR waves up to subcutaneous tissue resulted in lower optimum disinfection temperature, <70 °C in vogue. Thus, the combined UV-C and IR radiation is effective in killing the pathogenic bacteria and denaturing the glycoproteins.

1. Introduction

A global pandemic caused by severe acute respiratory syndrome coronavirus-2 (SARS-CoV-2) leading to a highly contagious disease called COVID-19 forced a complete lock-down in many countries. The virus is transmitted from aerosols and contacting surfaces [1]. This pandemic increased the usage of personal protective equipment (PPE) and sterilization devices to arrest the spreading of the disease. However, the disposal of PPE kits and other personal accessories created a huge amount of secondary contagious pollution. Moreover, the throwing of these infected kits and accessories to the environment contaminates the air and water systems. Conde-Cid et al. have recently confirmed the presence of SARS-CoV-2 in wastewater [2]. SARS-CoV-2 from wastewater can migrate to soil [3,4] affecting the planet and its ecosystem [5]. Thus, it is necessary to sterilize surfaces of daily usage as well as contaminated wastes. The design and development of a cost-effective sanitization device for sterilizing day-to-day life accessories is the need of the hour.

The SARS-CoV-2 comprises surface spike glycoprotein and Ribonucleic acid (RNA) [6]. The inactivation of the coronavirus is achieved through two approaches: (1) interfering with RNA or synthesized protein namely, antigen and (2) unfolding/denaturation of the spike protein [1]. The unfolding of the protein disables its binding with surface receptors, e.g., angiotensin converting enzyme 2 (ACE2) and entry into the host cells [7,8]. Approach 2 is mostly recommended as a preventive measure. For this, researchers have always emphasized the importance of sterilizers and different sterilization techniques [9–11]. The COVID-19 pandemic has further underlined the effective design and development of sterilization chambers with proper sterilization techniques [12–15]. Jacobs et al. thoroughly reviewed sanitization methods for filtering facepiece respirators and found that ultraviolet germicidal irradiation (UVGI) was the most widely used and effective for inactivating SARS-CoV-2 without reducing filtration efficiency [16]. Liao et al. studied the effect of five widely used user-friendly sterilization

* Corresponding author at: Department of Mechanical Engineering, Indian Institute of Technology Guwahati, Guwahati 781039, Assam, India.
E-mail address: uday@iitg.ac.in (U.S. Dixit).

https://doi.org/10.1016/j.ijbiomac.2022.08.197
Received 23 May 2022; Received in revised form 12 July 2022; Accepted 30 August 2022
Available online 3 September 2022

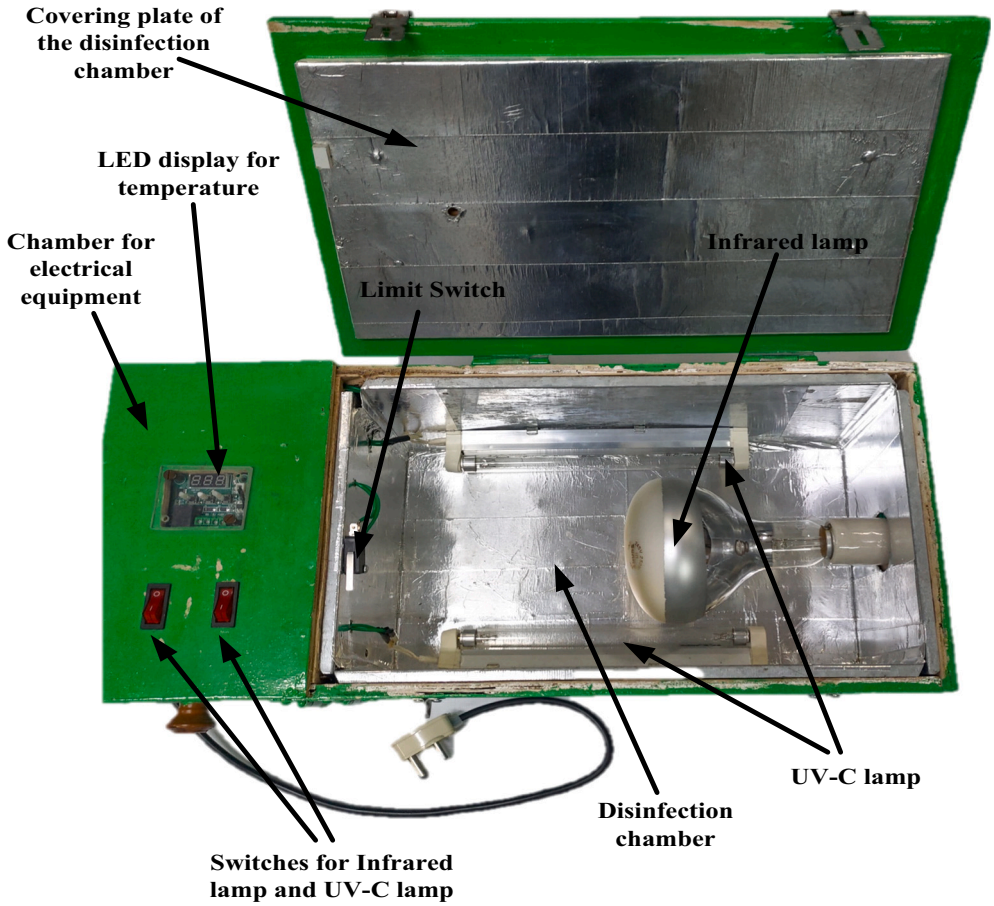

Fig. 1. Photograph showing different parts of the disinfection box.

techniques namely, (i) heat with humidity, (ii) steam, (iii) 75 % alcohol, (iv) household diluted chlorine-based solution and (v) UVGI on the filtration ability of face masks [13]. Each of these methods has its own merits and demerits. Ludwig-Begall et al. studied three sanitization techniques: (i) UVGI, (ii) vaporized hydrogen peroxide (H_2O_2) and (iii) dry heat to decontaminate filtering facepiece and surgical masks [14]. International Advanced Research Center for Powder Metallurgy and New Materials (ARCI), India, established physical, dry heat and chemical sanitization methods by using UVC lamps, honeycomb air heater and HOCl fogging systems, respectively, to combat COVID-19 [17]. Sabino et al. reported that UV-C light can be used to successfully deactivate SARS-CoV-1 and other RNA-based coronaviruses transmitted through liquid, air and other inanimate surfaces [18]. The UV-C radiation in the wavelength range of 250 nm to 270 nm is highly absorbed by the nucleic acids of microbial cells, which leads to microbial DNAs and RNAs damages. Thus, UV-C radiation becomes fatal to microorganisms [19]. Damit et al. used infrared (IR) radiation to disinfect fibrous filters contaminated with bioaerosols [20]. Molin and Östlund developed a device for the inactivation of spores using IR radiation [21]. The efficacy of UV-C based sterilization is affected by surface properties namely surface roughness. This method is more efficient on the smooth surfaces of kits, fruits and vegetables [22]. On the other hand, heating can kill or inactivate the pathogens even in an aqueous solution. Mahanta et al. studied the combined effect of heat and UV radiation for the prevention of COVID-19. The combination of UV radiation and heat was used for disinfecting day-to-day life small items like wallet, belt and wrist watches [15].

In addition, apart from inactivating the coronavirus, the disinfection boxes should be designed for the broad-spectrum of antibacterial activities. This can enable the multipurpose usage of disinfection boxes in healthcare. In this study, a disinfection box was designed and tested for its effectiveness in the killing of bacteria pathogens along with the unfolding of proteins. For the purpose of heating, IR radiation was set up in the disinfection box along with UV-C. IR based heating was preferred to other conventional heating because of many advantages such as high energy efficiency, more penetration depth, simple, uniform heating, lower heating time, higher heat transfer coefficients and compactness [23]. Optimization of UV-IR disinfection time and temperature were performed for the inactivation of bacterial growth on both a Gram-positive, namely, *S. aureus* and a Gram-negative, namely, *S. typhi* using a statistical tool response surface methodology with central composite design technique (RSM-CCD). Based on the obtained optimized conditions, the effect of treatment on the secondary structures of SARS-CoV-2 spike protein and another model protein RNase A was studied. RNase A is a structurally versatile and highly stable protein having 124 amino acid residues [24,25]. The main focus of the present work is to provide an inexpensive and efficient disinfection method by combining IR and UV-C irradiations to fight against contagious infections by viruses and bacterial pathogens.

2. Materials and methods

A cost-effective UV and IR heat based disinfection box was designed and fabricated. IR lamp manufactured by Sunny, India and UV-C lamps manufactured by Philips, Poland were used in this disinfection box. A Digital Temperature Controller (DTC) manufactured by Robocraze, India, was used to maintain the temperature inside the disinfection chamber. A timer manufactured by Selec 800XA, India, was used to turn off the disinfection chamber. Recombinant spike SARS-CoV-2 (catalogue # NR-52397) was procured from Biodefense and Emerging Infections

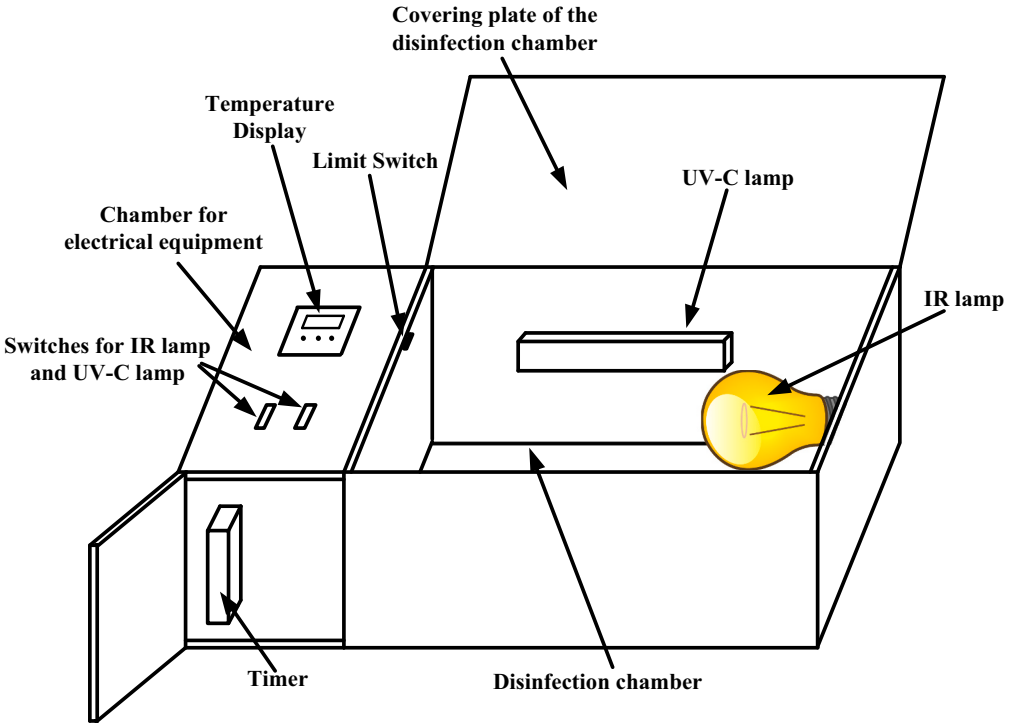

Fig. 2. A schematic diagram of the disinfection box.

Research Resources Repository (BEI Resource) free of cost for supporting research in COVID-19 disease and Bovine Pancreatic Ribonuclease A (catalogue # R6513) was purchased from Sigma Aldrich. Milli-Q water of resistivity 18 MΩ-cm at 25 °C was used for all the experimental studies.

2.1. Design of a UV and IR based disinfection chamber

The disinfection box consisted of a wooden box of size 53 × 24 × 21 cm^3, one 250 W infrared (IR) lamp, two 11 W UV-C lamps, one DTC and one timer. There were two parts of the wooden box, one part was used as a chamber for electrical equipment and the other part was used for disinfection purpose. A timer and electrical connections were placed inside the chamber of electrical equipment. IR lamp manufactured by Sunny, India, was used for heating purpose whereas UV-C lamps manufactured by Philips, Poland, were used for radiation. Two lightweight lamp holders made of aluminum were used to hold the UV-C lamps. Two separate electrical switches were used for turning on/off the IR lamp and UV-C lamps. A DTC manufactured by Robocraze, India, was connected with the IR lamp to maintain the temperature inside the disinfection chamber. DTC comprised two parts namely, a thermocouple to measure the temperature and an LED display to show the temperature. When the temperature inside the box crossed the temperature value already set in DTC, it would automatically stop heating by turning off the IR lamp. As soon as the temperature inside the box lowered by 2 °C with respect to the set value, DTC would turn on the heating source i.e. IR lamp. A timer manufactured by Selec 800XA, India, was connected with the main supply in such a way that it would turn off the disinfection chamber after a pre-decided time duration for disinfecting an item. A limit switch was placed on the top cover to protect the human eye and skin from direct exposure to UV radiation. A high reflecting Galvanized iron (GI) sheet was used inside the disinfection chamber to cover the inner surfaces of the wooden box for the prevention of heat loss through the walls of the box. The thin air layer between the GI sheet and the surfaces of the wooden box acted as a thermal insulator. Fig. 1 and Fig. 2 show the photograph and a schematic diagram of the box, respectively. The disinfection box was designed in such an effective way that it took only 70 s for an empty box to achieve a temperature of 70 °C from an ambient temperature of 25 °C. Further, once the temperature inside the chamber reached to a set temperature of T °C from room temperature, Digital Temperature Controller (DTC) maintained the temperature at $T \pm 1$ °C inside the chamber for a given period of the experiment. The temperature at the center of the disinfection chamber (where items to be disinfected were kept) was also measured using a thermometer and no difference was found compared to the temperature measured by Digital Temperature Controller (DTC).

Table 1
Material cost in the fabrication of a disinfection box.

S. N.	Item	Quantity	Unit cost ($)	Total cost ($)
1	11-W UV-C Lamp	2	3.28	6.56
2	UV-C Lamp holder	2	2.76	5.52
3	250-W IR Lamp	1	6.57	6.57
4	IR Lamp holder	1	0.66	0.66
5	Electrical switches	2	0.20	0.40
6	Digital Temperature Controller (DTC)	1	2.76	2.76
7	Timer	1	9.85	9.85
8	Limit switch	1	0.46	0.46
9	8 mm thick plywood of surface area 6026.5 cm^2			3.86
10	0.8 mm thick GI sheet of surface area 4073.94 cm^2			2.25
11	Miscellaneous			1.97
	Total			$40.86

UV-C radiation required to inactivate SARS-CoV was suggested to be above ~3.6 J/cm^2 [13]. UV-C dose can be calculated using [26].

$$D \propto \frac{Pt}{4\pi d^2} \quad (1)$$

where D is UV-C dose, P is UV bulb power, t is exposure time and d is distance of bulb from the surface to be sterilized. Using Eq. (1), UV-C dose provided to the items to be disinfected in this disinfection box

Table 2
The experiment sets designed by RSM-CCD with predicted and obtained responses for *S. aureus* and *S. typhi* antibacterial study.

	Time (min)	Temp. (°C)	*S. aureus*				*S. typhi*			
			Growth inhibition in dye (%)		Cell viability (log CFU/mL)		Growth inhibition in dye (%)		Cell viability (log CFU/mL)	
			Expt.	Pred.	Expt.	Pred.	Expt.	Pred.	Expt.	Pred.
1	10	40	0.59	2.33	4.31	4.21	20.54	19.90	4.63	4.45
2	6.46	44.39	6.11	7.36	4.26	4.37	14.37	18.06	4.48	4.57
3	13.54	44.39	9.47	6.64	4.18	4.28	24.84	23.23	4.07	4.27
4	10	55	8.75	9.71	4.18	4.18	27.31	26.89	3.97	3.96
5	10	55	11.07	9.71	4.18	4.18	24.70	26.89	3.95	3.96
6	10	55	9.60	9.71	4.19	4.18	27.18	26.89	3.94	3.96
7	10	55	8.93	9.71	4.18	4.18	29.50	26.89	3.95	3.96
8	15	55	31.81	33.21	3.94	3.81	43.55	45.30	3.90	3.75
9	5	55	14.23	9.85	4.24	4.09	23.77	18.03	4.02	4.02
10	10	55	10.18	9.71	4.18	4.18	25.73	26.89	3.95	3.96
11	13.54	65.61	55.94	57.66	2.30	2.47	72.21	72.49	2.60	2.66
12	6.46	65.61	18.06	23.87	2.60	2.78	33.48	39.05	2.78	2.74
13	10	70	54.78	50.07	2.00	1.81	72.88	69.56	2.00	2.02

Note: Expt. →Experimental, Pred.→Predicted, Temp.→Temperature.

was calculated as 11.11 J/cm^2 (assuming a proportionality factor of 1 in Eq. (1)), which was found to be more than the dose suggested [13].

Items used in fabricating the disinfection box are listed in Table 1. An amount of US $40.86 was the material cost for fabricating one unit of disinfection box. Considering the present Indian scenario, the labour cost for fabricating one unit of disinfection box was estimated as $13.13. Thus, the total cost was calculated as $53.99 for fabricating one unit of disinfection box. This cost will further reduce in mass production. Online shopping portals delivered UV-C based disinfection systems of similar size at a price range of $98–183. Thus, the proposed disinfection box is economical compared to those available in online shopping portals. In addition, the proposed disinfection box has IR radiation heating facility along with UV-C radiation facility.

2.2. Design of experimental conditions

The experimental design to explore the effect of UV-IR treatment on bacterial growth was performed using RSM-CCD tool in Design-Expert (ver 7.0). A range of UV disinfection time (5 to 15 min) and IR mediated temperature (40 to 70 °C) were selected as input parameters for the RSM-CCD model to analyze the main and interaction effects on antibacterial activity [15]. The RSM-CCD model suggested a set of 13 experimental runs to predict the optimum time and temperature responsible for significant antibacterial action. Among these five experiments were replicate experiments. To examine the bacterial growth inhibition, the bacterial cells were subjected to tabulated UV-IR irradiation time and temperatures (columns 2 and 3 of Table 2). The output response was evaluated as the percentage of bacterial growth inhibition after disinfection treatment in comparison to the untreated (positive control) condition. The multiple regression analysis provided optimized and statistically significant solutions using two-way analysis of variance (ANOVA).

2.3. Antibacterial effect of UV-IR treatment

The antibacterial effect of temperature and heat was investigated on Gram-positive bacteria, *Staphylococcus aureus*, and Gram-negative bacteria, *Salmonella typhi*. The bacteria were initially enriched overnight in Nutrient broth (N.B., catalogue # M002) using a shaker incubator maintained at 180 rpm and 25 °C and further sub-cultured in the same medium for 6 h to obtain cells in the early log phase. The culture was centrifuged at 5000 rpm for 5 min and bacteria were resuspended in sterile water to obtain the optical density (O.D.) value of 0.1 corresponding to bacterial concentration of 10^7 CFU/mL. Thus, obtained bacterial suspension was aliquoted to a 5 mL glass test tube and subjected to UV-IR treatment. After treatment, the viability of cells was determined using the colourimetric, agar spread plate and microscopy.

2.3.1. Colourimetric assay

For the colourimetric bacterial cell viability determination, a resazurin dye (catalogue # RM125) assay was performed. The assay uses colourimetric redox dye, which changes the colour from blue (A_{600} absorbance) in the oxidized form to pink colour when reduced (A_{570} absorbance) due to the formation of resorufin [27–29]. For the assay, an equal volume of resazurin dye (67.5 mg/L) was mixed with treated bacterial suspension and incubated statically at 37 °C under dark for 4 h. After incubation, the samples were spectrophotometrically measured at 570 nm and 600 nm. A similar experiment was performed using untreated bacterial suspension as a positive control. The bacterial growth inhibition was calculated using [30].

$$G_i = \left\{ \frac{(A_{570} - A_{600}R_0)_{untreated} - (A_{570} - A_{600}R_0)_{treated}}{(A_{570} - A_{600}R_0)_{untreated}} \right\} \times 100 \quad (2)$$

where G_i is percentage growth inhibition. R_0 was calculated as a correction factor (A_{570}/A_{600}) using only dye in water as a sample.

2.3.2. Agar spread plate assay

In addition, the spread plate technique was performed using treated bacterial suspension to evaluate the bacterial viability after disinfection treatment. For this, the treated bacterial suspension was serially diluted five times in sterile water and 50 μL of 10^{-5} dilution was spread plated on nutrient agar (NA), and incubated overnight at 37 °C [15]. The concentration (CFU/mL) of viable bacteria was determined using

$$CFU \Big/ mL = \frac{ND_i}{V} \quad (3)$$

where N is number of bacterial colonies, D_i is dilution factor and V is volume plated (in mL). An untreated bacterial suspension was also serially diluted and spread plated as a positive control. The percentage growth inhibition was calculated from

$$G_i = \frac{CFU/mL_{untreated} - CFU/mL_{treated}}{CFU/mL_{untreated}} \times 100 \quad (4)$$

2.3.3. Surface morphology of treated bacteria

The effect of UV-IR treatment on bacterial viability was further evaluated using field emission scanning electron microscopy (FESEM) (model Sigma, make Zeiss). The bacteria were treated under optimized temperature and disinfection time and later drop casted on C tape [31]. Krishnamurthy et al. carried out microscopic and spectroscopic analyses to explore the damage of *Staphylococcus aureus* treated with pulsed UV light and IR heating [32]. Cell wall damage and cellular content leakage

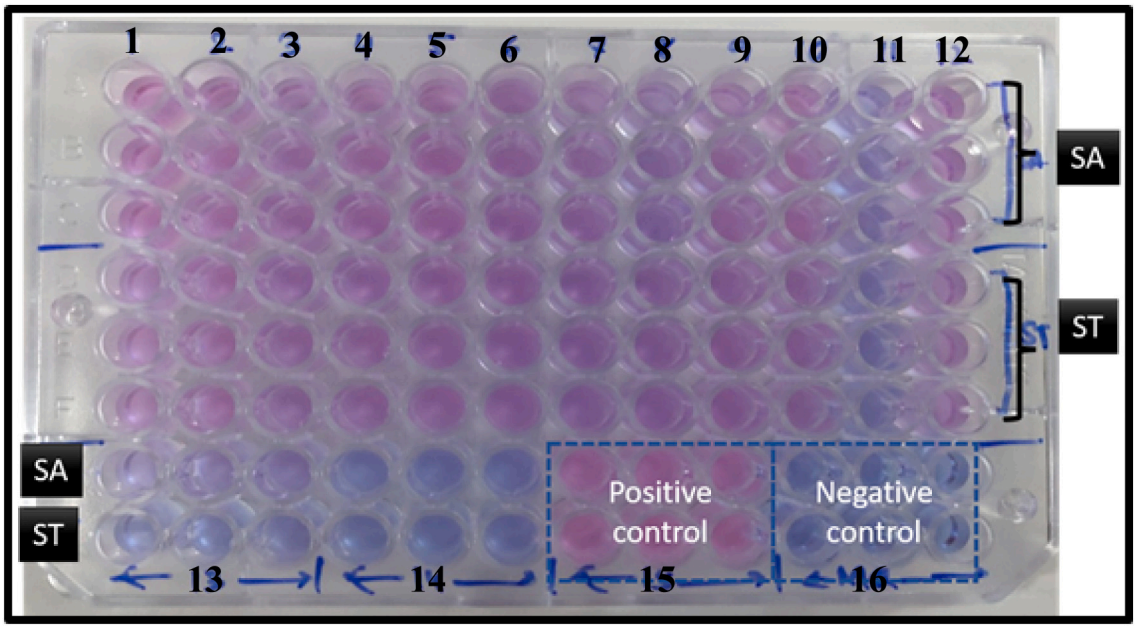

Fig. 3. Colourimetric assay of bacterial growth inhibition in the presence of UV-IR treatment at RSM-CCD suggested experimental conditions (1 to 13) using Resazurin dye [SA: *S. aureus*; ST: *S typhi*; well no. 14: previously optimized treatment conditions of UV-C and dry heat at 70 °C for 15 min; well no. 15: positive control (untreated bacterial suspension in dye) and well no. 16: negative control (only dye in sterile water)].

confirmed the inactivation of bacteria. In this work, microscopic evaluation was carried out to analyze the change in the bacterial morphology due to the inactivation using UV-C and IR heat.

2.4. Effect of UV-IR heat treatment on proteins

Aqueous solutions of spike and RNase A proteins were exposed in the IR and UV-C treatment box. The samples were collected and the secondary structure determination was performed through intrinsic fluorescence, FTIR and CD spectroscopy.

2.4.1. Protein sample preparation

An amount of 0.45 μM Recombinant SARS-CoV-2 spike protein was prepared from the stock solution of 0.57 μM in Trish HCl buffer. The recombinant SARS-CoV-2 spike protein was packed in vials and it is used as it is from the stock. 72 μM stock solution of RNase A was prepared in 10 mM PBS buffer and checked its concentration under UV absorbance at 280 nm [33]. Its concentration was determined from Beer-Lambert's law using an extinction coefficient of ~9727 M^{-1} cm^{-1}. For the IR treatment studies, (36 μM) 0.5 mg/mL working solution was prepared.

2.4.2. Secondary structure analysis of proteins

2.4.2.1. FTIR spectroscopy. Fourier transform infrared (FTIR) spectroscopy was performed using the FTIR instrument from (Shimadzu IR Affinity S1). A sample solution of 2 μL was added on top of the ZnSe crystal. For the entire investigation, a minimum of 64 scans and a resolution of 4 cm^{-1} were preset and spectra were recorded in the full range of 400–4000 cm^{-1}. The protein sample was prepared in a buffer solution. Thus, the buffer was recorded as the background spectra which was automatically subtracted from the sample spectra. The CO_2 and moisture corrections were also performed by the instrument. Further, the amide-I region (1600–1700 cm^{-1}) of the spectrum was resolved, deconvoluted and fitted with Gaussian curves using Origin 8.5 software [34–36].

2.4.2.2. CD spectroscopy. Far UV-CD spectroscopic measurement was performed using a circular dichroism (CD) spectrophotometer (JASCO, J-1500) to investigate the change in the secondary structure of UV-IR treated protein sample. A quartz cuvette of 0.1 cm path length was used for this study. The spectra were collected in the range of 260–190 nm [37–40]. Samples were scanned as an average of 5 accumulations with a scan speed of 100 nm/min and at 0.1 nm bandwidth. The spectrum of the buffer was used for the baseline correction prior to the measurement of the samples. A sample of 0.2 mg/mL concentration was prepared for the reading. The machine CD signal value θ in millidegree (mdeg) has been converted to mean residue ellipticity value (MRE) in deg. cm^2 $dmol^{-1}$ $residue^{-1}$.

2.4.2.3. Tryptophan intrinsic fluorescence. The alternation in the secondary structure was also correlated with the intrinsic fluorescence of aromatic amino acids. The native and treated samples of spike protein were diluted in Tris buffer to prepare 1 mL of 0.01 μM solution. The native and the treated spike protein solutions were then loaded in a quartz crystal cuvette to check the change in intrinsic fluorescence using a Fluoromax 4 spectrofluorometer (Horiba Scientific). The excitation wavelength was set at 290 nm. A 5 nm excitation and emission slit width was fixed and an average of five scans was accumulated for all the readings.

3. Results and discussion

In this study, a simple, easy to handle and low cost disinfection box is fabricated and the synergistic effect of UV-C and IR heat over sanitization was investigated. For this purpose, the effect of UV-C and IR heat sanitization was performed, and its effect on the bacterial cells namely, *S. aureus* and *S. typhi* and also on two proteins namely, whole spike protein and RNase A was checked. The detailed results are described in the sequel.

3.1. Effect of IR heat and UV treatment on bacterial cells

Temperature and UV irradiation time have shown significant inhibitory effects on bacterial growth, as previously established in our study [15]. It was reported that only heat or only UV may injure the cell but may not kill them, increasing the chance of their revival and hence

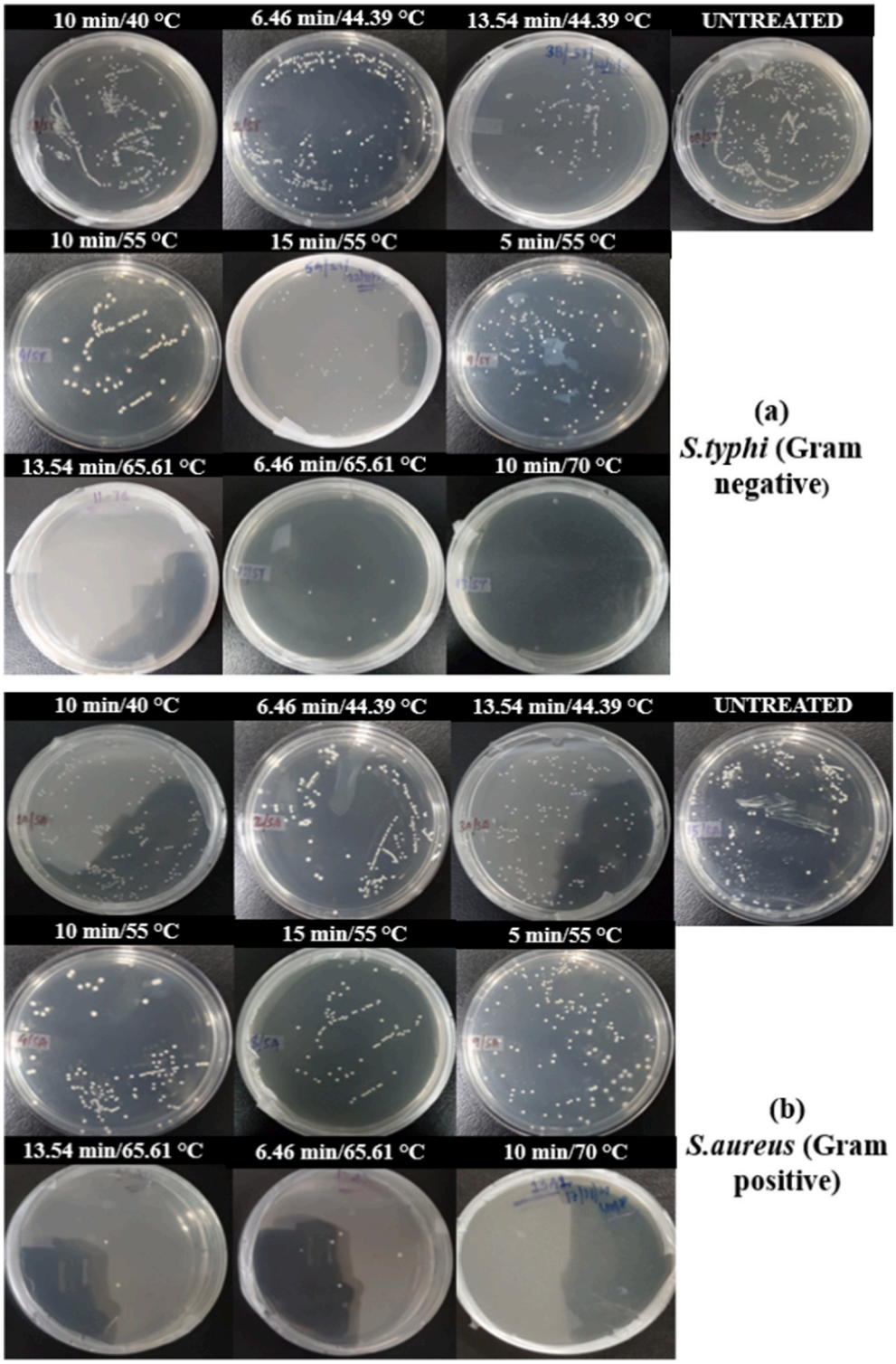

Fig. 4. Bacterial growth inhibition study using serial dilution (5 times) and agar spread plate technique at various RSM-CCD experimental conditions against (a) Gram-negative (*S. typhi*) and (b) Gram-positive (*S. aureus*).

pathogenicity. Thus, simultaneous UV-heat treatment using IR irradiation was explored for disinfection in this study. Colourimetric technique [30] and spread plate technique [15] were used to study antibacterial activities against both *S. aureus* and *S. typhi*. Temperature and disinfection time were considered as independent variables and various combinations, as suggested by the RSM-CCD optimization design, were investigated to achieve maximum growth inhibition of bacteria (response). Table 2 lists the 13 sets of experimental runs designed by RSM-CCD and their respective experimental and predicted responses. For 5 replicate experiments, coefficient of variation in cell viability was 1 % and 2.5 % for *S. aureus* and *S. typhi*, respectively.

In the case of the colourimetric assay, the viable bacteria utilize the available oxygen resulting in the reduction of the dye (Resazurin). This leads to a change in the colour of the dye from blue to pink. Fig. 3 shows the colourimetric change in the dye due to the occurrence of reduced culture conditions in the presence of live bacterial cells treated under

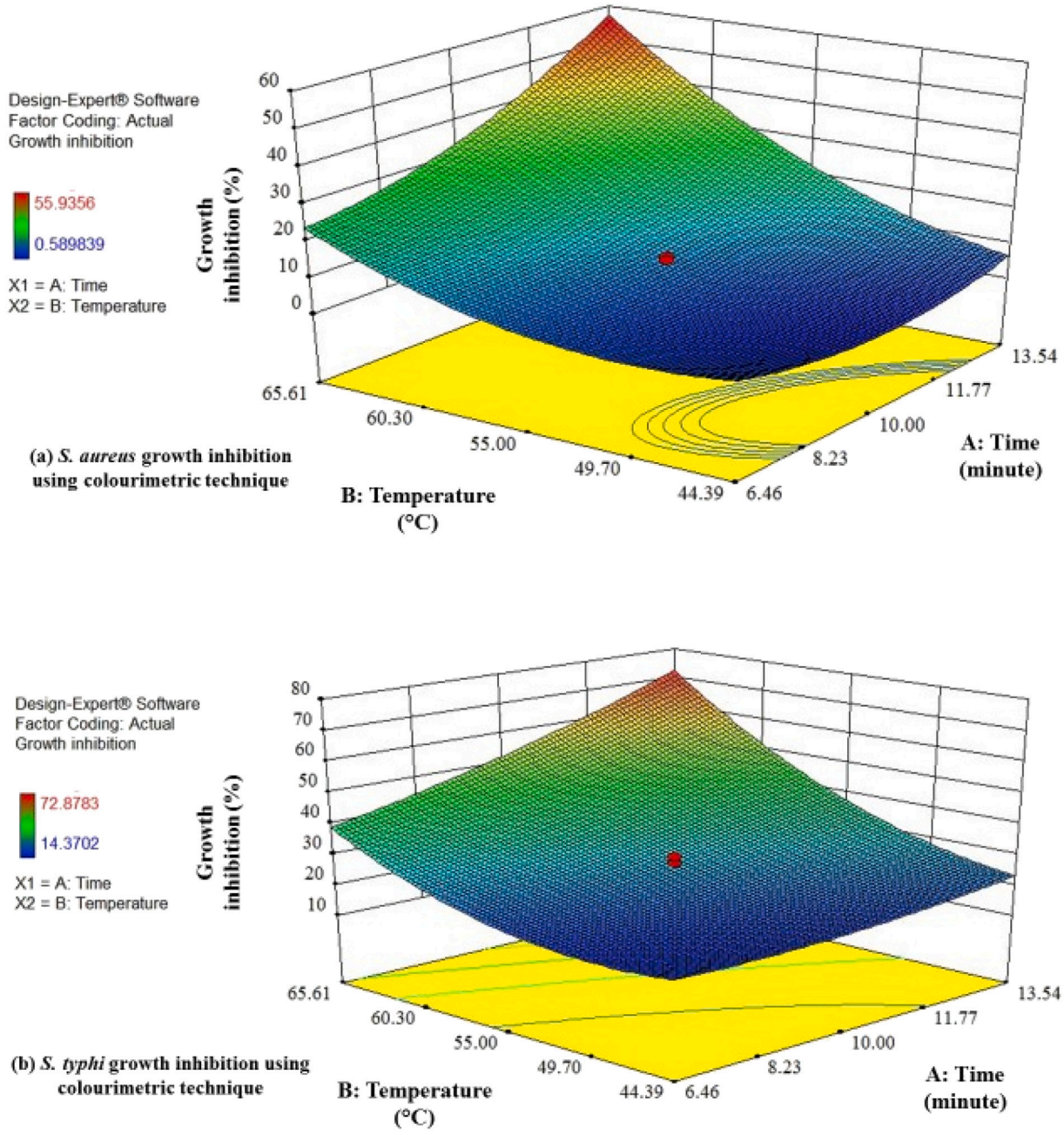

Fig. 5. Contour 3D response surface plots showing bacterial growth inhibition using colourimetric technique in (a) *S.aureus* and (b) *S.typhi* considering Temperature and UV irradiation time as the variable input parameters.

various conditions as listed in Table 2. The experiments were performed in triplicates and SA represents *S. aureus* while ST refers *S. typhi*. The presence of blue colour in the microplate well numbers 11 and 13 suggested the inactivation of bacteria under treatment conditions of 13.54 min at 65.61 °C and 10 min at 70 °C, respectively, leading to an insignificant change in dye colour than the control. The positive control (wells 15) represented untreated bacterial viability showing a complete pink colour whereas the negative control indicated the original blue colour of dye in sterile water. Thus, lesser pink colouration suggested a decrease in cell viability and an increase in growth inhibition due to disinfection treatment. In addition, well number 14 represented disinfection at the previously optimized treatment conditions (UV-C and dry heat) of 15 min at 70 °C [15]. This suggested that the present IR heating and UV treatment are more effective in achieving growth inhibition within 13.54 min at a comparatively lesser temperature of 65.61 °C. The better disinfection by IR irradiation is due to its larger penetration depth. The IR waves can penetrate up to subcutaneous tissues (1–4 mm), while UV and visible light penetrate up to epidermis (≤200 μm) and dermis (200–1500 μm) layers, respectively [41]. Further, the power density of IR irradiation was estimated as 3.18×10^4 W/m^2, which effectively inactivated bacterial pathogens. Damit et al. reported the inactivation of *E. coli* and *B. subtilis* spores with IR irradiation of a power density of 2.0×10^4 W/m^2 [20].

In addition, the inhibition of bacterial growth was monitored by spread plate techniques. The treated bacterial suspension was serially diluted five times and plated on NA plates, and visible colonies were counted after 12 h of incubation. The untreated bacterial suspension was also plated under 5 times dilution, and colonies were counted as a positive control. The cell viability for control (untreated) was obtained as 2.5×10^4 and 6.5×10^4 CFU/mL for SA and ST, respectively. Fig. 4

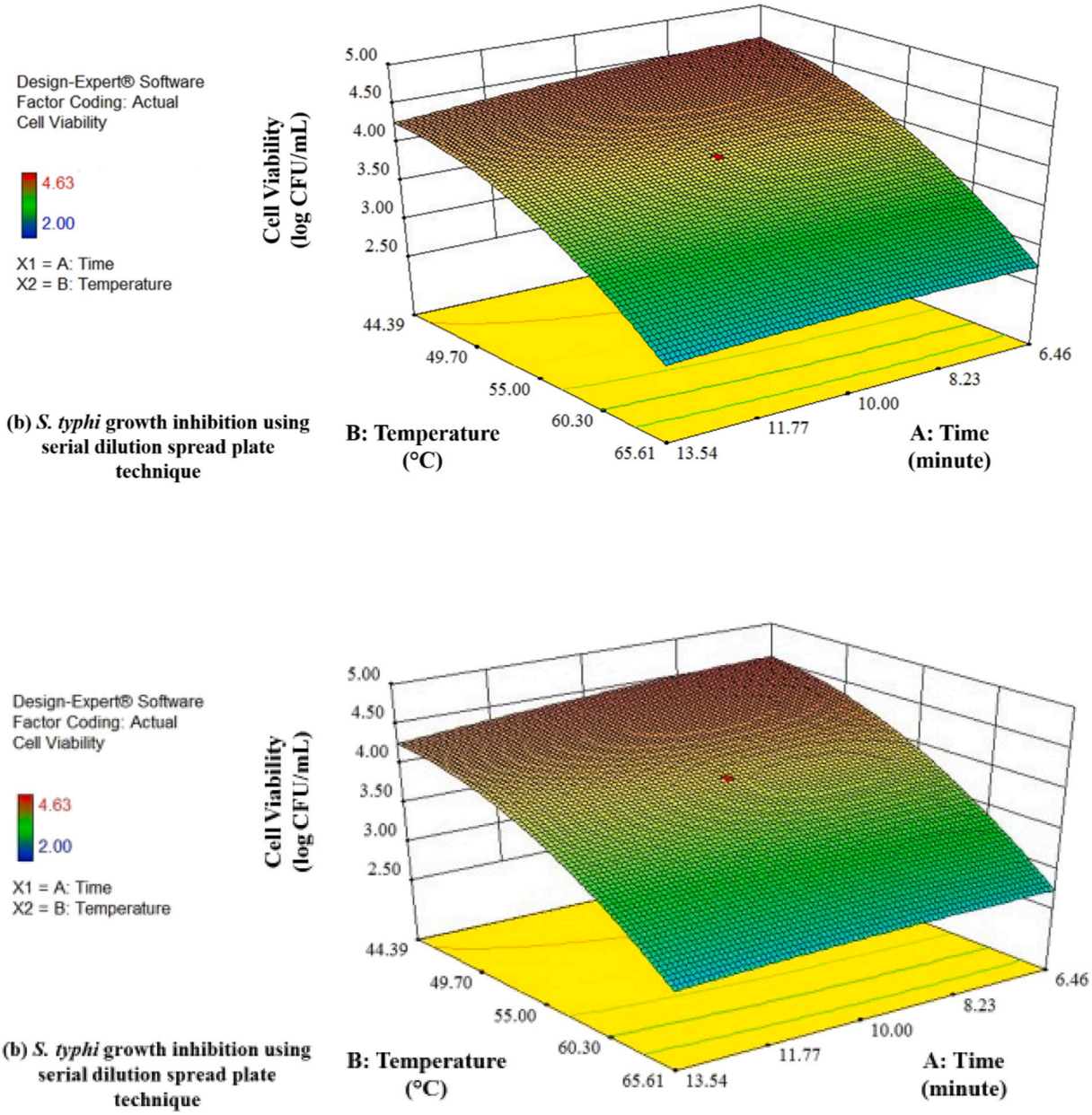

Fig. 6. Contour 3D response surface plots showing bacterial growth inhibition using serial dilution spread plate technique in (a) *S. aureus* and (b) *S. typhi* considering; Temperature and UV irradiation time as the variable input parameters.

Table 3
RSM-CCD Quadratic model fitting to the experimental parameters with ANOVA analysis.

Bacteria pathogen	Quadratic polynomial eq. (*A*: Time; *B*: Temperature)	ANOVA analysis
S. aureus	$9.71 + 8.26A + 16.88B + 8.62AB + 5.91A^2 + 8.24B^2$	*A, B, AB,* A^2, B^2 are significant model terms. ($R^2 = 0.97$)
S. typhi	$26.89 + 9.64A + 17.56B + 7.05AB + 2.39A^2 + 8.92B^2$	*A, B, AB,* B^2 are significant model terms. ($R^2 = 0.97$)

shows the cell viability for various treatment conditions. The decrease in the number of colonies indicated the effectiveness of sterilization. >95 % of bacterial growth inhibition was obtained for the combined IR and UV irradiation at temperature ≥ 65.61 °C and time ≥ 10 min for both the SA (≤2 × 10^2 CFU/mL) and ST (≤4 × 10^2 CFU/mL) bacteria. These results are in concordance to the disinfection effects observed from colourimetric assay.

Fig. 5 and Fig. 6 show 3D contour response surface plots describing the percentage of bacterial growth inhibition in the range of disinfection temperature and time chosen for this study. The obtained responses were fitted to quadratic polynomial equations as mentioned in Table 3. Both response factors fitted well to quadratic model equations and predicted responses are also listed in Table 2. The ANOVA was performed for the statistical analysis. The coefficient of determination (R^2) values of experimental and predicted data were found to be ≥0.94. The *p*-value of ≤0.001 indicated the fitness of the quadratic model equations. Both the time and temperature of UV-IR irradiation were found to be significant for bacterial growth inhibition. The optimized condition for the maximum inhibition of bacterial growth in the given range of input variables was predicted to be 65.61 °C of temperature for 13.54 min.

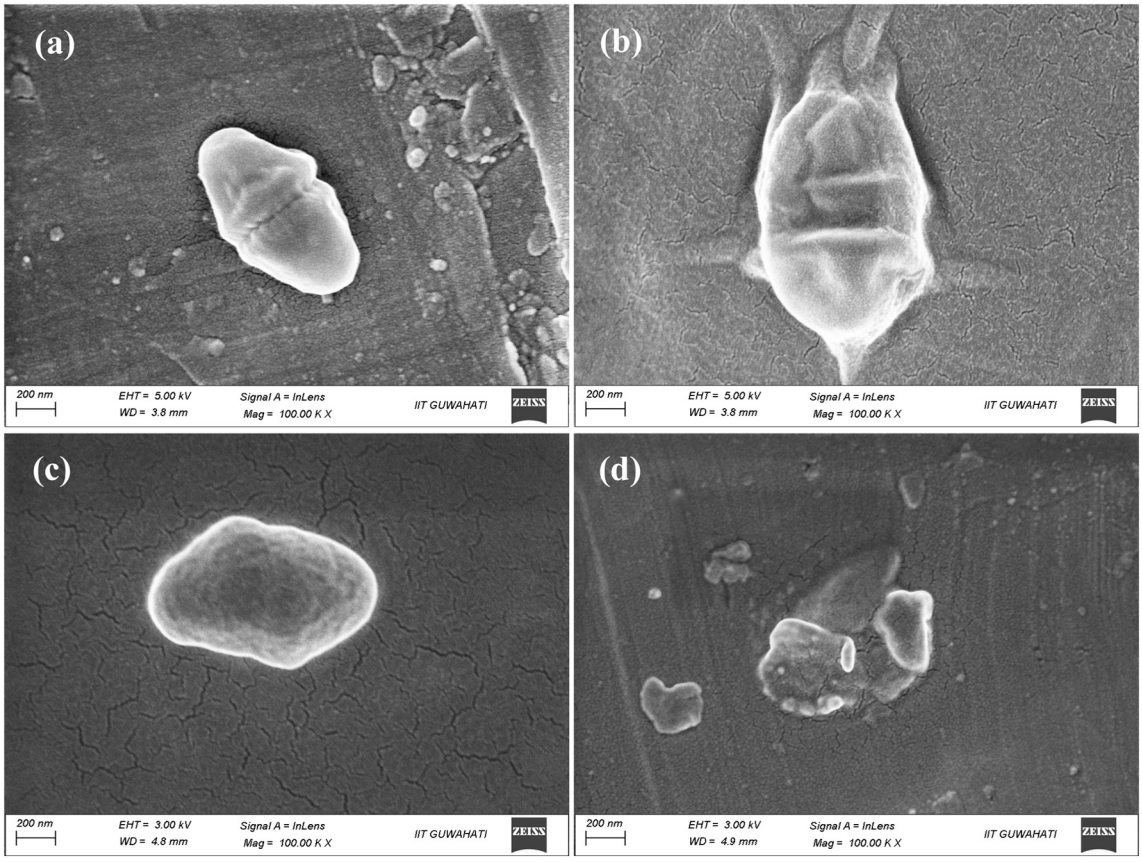

Fig. 7. Microscopic evaluation (X10^5) of (a) *S. aureus* control sample (b) *S. aureus* sample treated to combined UV-C and IR heat showing cell wall breakage (c) *S. typhi* control sample (d) *S. typhi* sample treated to combined UV-C and IR heat showing cell wall breakage (1-mL sample was treated at 65.61 °C for 13.54 min).

3.2. Microscopic evaluation of bacterial cell using FESEM

The killing of bacterial pathogen occurs via multiple routes like rupture of cell membrane, inactivation of genetic materials/proteins and interfering with cell division. Calderon-Miranda et al. reported that pulsed electric fields (PEF) inactivated the microorganisms by affecting the cells physiology and morphology namely, dielectric damage of the cell wall, leakage of cellular material, cytoplasmic clumping, increase in cell wall roughness and fracture of the cell walls and cell membranes [42]. Liu et al. reported that chitosan treated *S. aureus* were inactivated by disrupting the membrane of dividing cells along with leakage of cell contents [43]. In this work, the synergistic effects of UV-C and IR heat treatment on *S. aureus* and *S. typhi* were analyzed on cellular morphology. The microscopic evaluation of the combined UV-C and IR heat treated *S. aureus* and *S. typhi* was carried out using FESEM. The morphologies (images) of untreated and treated *S. aureus* and *S. typhi* are shown in Fig. 7. Sample of 1 mL from each bacteria was treated at 65.61 °C for 13.54 min in the designed disinfection chamber. Microscopic analyses of *S. aureus* and *S. typhi* cells indicated the damage of cell wall integrity (rupture of cell wall) due to the combined UV-C and IR heat treatment. In control samples, cell walls have definite boundaries as shown in Fig. 7(a) and (c). However, treated samples have broken boundaries as the cell walls were destroyed (Fig. 7(b) and (d)). These observations indicated the effectiveness of the designed chamber for the killing of bacterial pathogens by disrupting the cell walls.

3.3. Effect of IR heat and UV treatment on the unfolding of the spike protein and RNase A

The disinfection process is frequently being followed to inactivate the novel coronavirus. Unfolding or change in conformation of the surface glycoprotein of a virus can lead to its disintegration and inactivation [1]. Thus, heating is one of the disinfection methods, which unfolds/denatures the virus spike protein and thus inactivates the virus. It has been reported that a high temperature of 70 °C leads to the loss of viral surface protein, disintegrating the viral assembly [1,15,44]. In this work, the effect of UV-C and IR heating has been tested on two important proteins: SARS-CoV-2 spike protein and RNase A. The virus spike protein mainly aids in the attachment and entry of the coronaviruses inside the host cells. It is a homotrimer where the S1 part is partly exposed to the outer environment and the S2 domain is partly immersed inside the lipid bilayer of the viral envelope [45]. RNase A is a very stable protein and is used as a model protein for studying the unfolding-refolding process [46]. The proteins in an aqueous solution were exposed inside the designed IR treatment box at the optimized conditions of 65.61 °C for 13.54 min as discussed in the earlier sections. The unfolding of proteins was analyzed by measuring the changes in the secondary structure and intrinsic fluorescence.

Fig. 8(a) and Fig. 8(b) show the FTIR spectra in the amide I region of native and treated spike protein. The spectra were deconvoluted and respective peak area were used to determine the contents of the secondary structure. The major peaks in the range of 1620–1635, 1642–1645, 1651–1655 and 1665–1685 cm^{-1} correspond to β-sheet, random coil, α-helix and β-turn, respectively [47]. The native spike protein contained 16.4 ± 0.5 % of α-helix, 34.7 ± 0.8 % of β-sheet, 28.9 ± 0.9 % of β-turn and 14.0 ± 2.0 % of random coil. These data correlate well with the literature reported by others [7,48,49]. However, post heat treatment, the contents of β-sheet increased to 43.7 ± 1.1 %, while α-helix decreased to 11.9 ± 1.5 %. This indicated the unfolding of spike protein after the heat treatment at 65.61 °C for 13.54 min in the designed chamber. Rath and Kumar studied the effects of different temperatures on the spike glycoprotein by molecular dynamics

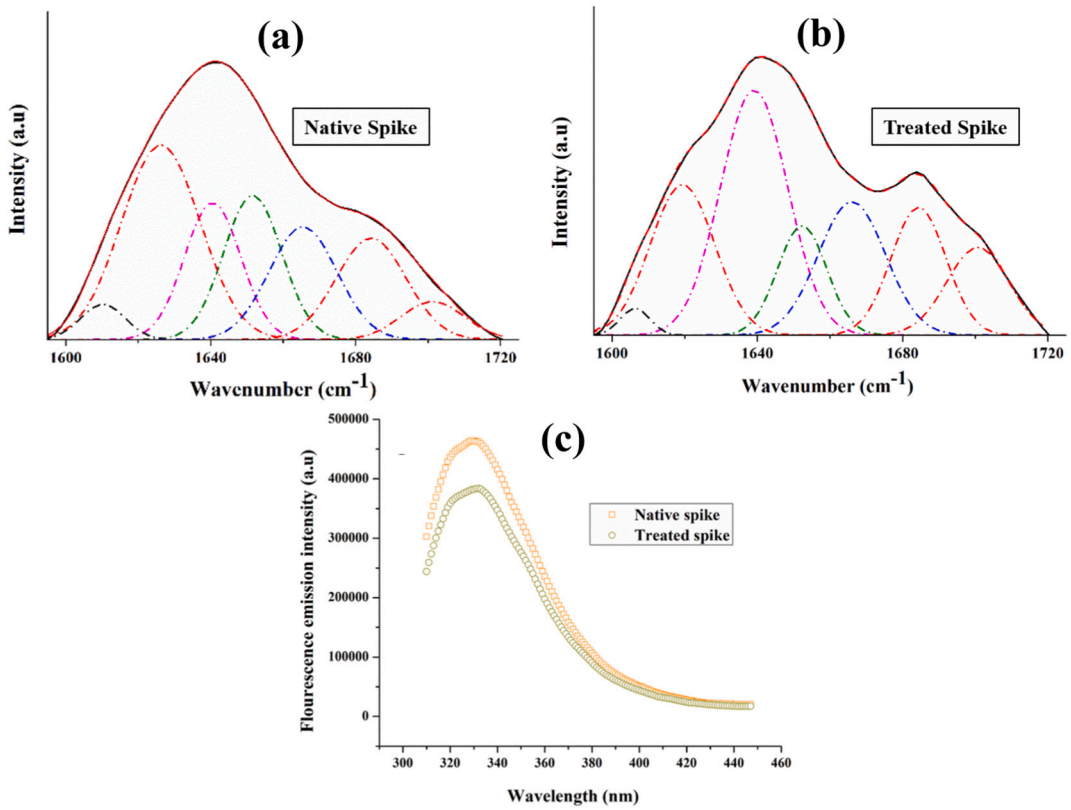

Fig. 8. Deconvulated second derivative spectra of (a) native spike; (b) treated spike and (c) intrinsic tryptophan fluorescence for native spike and IR and UV-C treated spike protein.

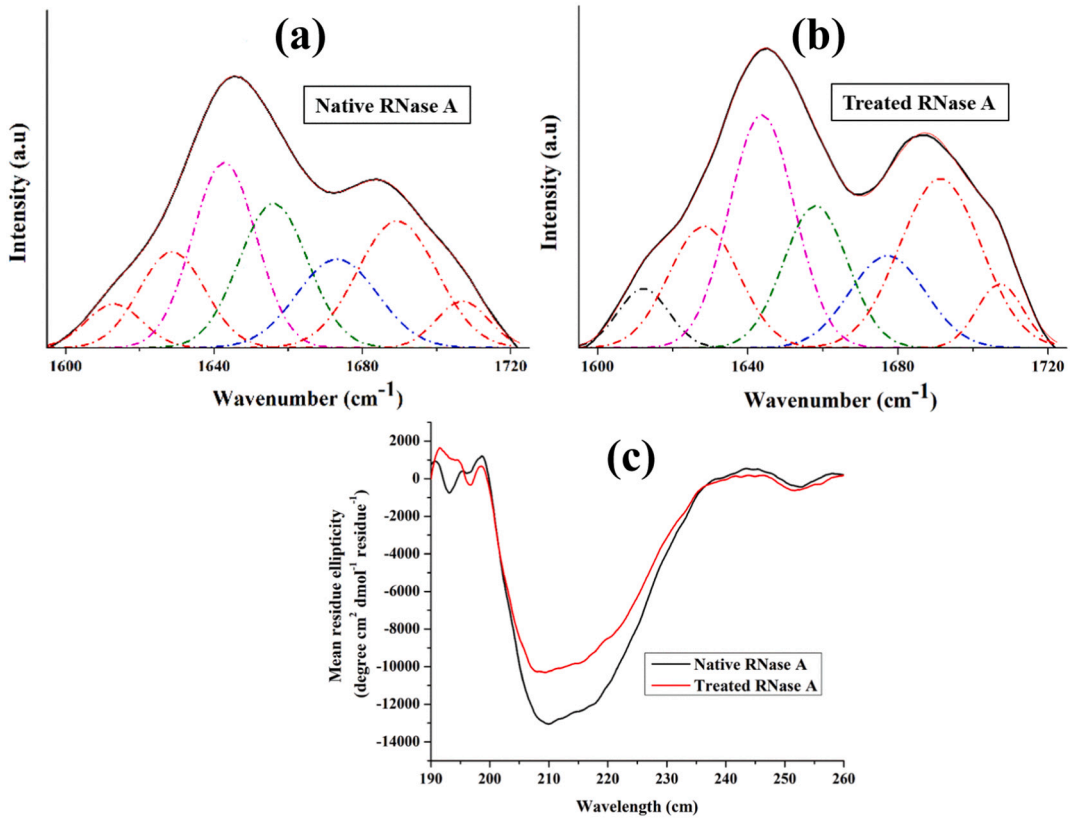

Fig. 9. Deconvulated second derivative spectra of (a) native RNase A; (b) treated RNase A and (c) Far-UV CD spectra of the native and IR-UVC treated RNase A enzyme.

simulation [45]. It was reported that at temperatures ≥50 °C (particularly at 70 °C), the receptor-binding domain (RBD) was found to get closed. The RBD is a part of S1 unit of spike protein and binds to the ACE2 (angiotensin-converting enzyme 2) receptor of the host protein. The unfolding of RBD stops the attachment of the spike protein to the host and thus inhibits the transmission of the virus [45,50].

In Fig. 8(c), FTIR data were correlated with the intrinsic fluorescence of the spike proteins. The intrinsic fluorescence is contributed by the presence of aromatic amino acids. Any alternation in the secondary structure of a protein interferes with the fluorescence intensity due to the reorganization of aromatic amino acids which results in the change of the microenvironment of the protein [51]. A decrease in the fluorescence intensity was observed for the treated spike protein as compared to the native protein (Fig. 8(c)). A decrease in tryptophan fluorescence indicated that there is an exposure of some of the tryptophan residues because of IR and UV-C radiations [52]. This resulted in an early quenching of the fluorescence as compared to the native spike protein.

Fig. 9(a) and Fig. 9(b) show the deconvoluted second derivative FTIR spectra in the amide 1 region of the native and treated samples of RNase A, respectively. RNase A contained 19.8 ± 1.0 % of α-helix, 37.5 ± 1.5 % of β-sheet, 14.3 ± 1.0 % of β-turn and 23.5 ± 0.9 % of random coil. Similar to the spike protein, the heat treatment using IR and UV-C irradiations resulted in the unfolding. The contents of α-helix decreased to 16.2 ± 1.3 % and in turn β-sheet increased to 42.5 ± 1.0 % after the treatment. Stelea et al. reported the distinct changes in the FTIR spectra of RNase A in the temperature range of 50 to 70 °C [53]. Also, the unfolding of RNase A protein was analyzed using CD spectroscopy. Fig. 9 (c) shows the CD spectra of native and treated RNase A protein. A decrease in the negative dip at 208 nm indicated the reduction in the contents of α-helix [53]. Therefore, the combined UV-C and IR radiations have shown the ability to kill the bacteria and also effectively denature the glycoproteins. The IR radiation is found to lower the polarization of C═O bonds (carboxylic groups) and thus weaken the hydrogen bonds [54]. The breaking and making of hydrogen and other intermolecular interactions leads to the unfolding of proteins [55,56].

4. Conclusion

Considering the global pandemic caused by COVID-19, a disinfection box equipped with both UV-C radiation and IR heating facility was designed and tested for antibacterial and antiviral activities. An IR lamp of 250 W and two 11 W UV-C lamps were the most important parts of the box for disinfection purposes. The broad-spectrum antibacterial activity was tested against Gram-positive namely, *S. aureus* and Gram-negative namely, *S. typhi* and antiviral ability was accessed through the unfolding of SARS-COV-2 spike glycoprotein. Experiments were carried out to optimize the time and temperature for the effective disinfection against the above mentioned bacteria and virus. Small day-to-day life items namely belt, wallet, wrist watch, mask can be disinfected in the optimized conditions. The designed box can be used for the disinfection of contagious hospital wastes before their disposal. The salient observations and recommendations are as follows:

i. The overall observations suggested that combined IR and UV-C irradiations together at 65.61 °C for 13.54 min was sufficient to kill both Gram-positive (*S. aureus*) and Gram-negative (*S. typhi*) bacteria along with inactivation of spike and RNase proteins. This temperature is lower than 70 °C used in visible light and UV-C radiation due to larger penetration depth of IR irradiation up to subcutaneous tissues (1–4 mm).
ii. The microscopic evaluation confirmed the cell wall damage that further led to the killing of treated bacteria.
iii. Change in secondary structures in spike protein was investigated by FTIR and intrinsic fluorescence, which confirmed the decrease in helicity and increase in β-sheets. In the case of RNase A, FTIR and CD confirmed the unfolding.
iv. The present study confirmed the suitability of the designed low-cost disinfection box based on UV-C and IR radiations for effective disinfection.

CRediT authorship contribution statement

Nilkamal Mahanta: Investigation, Methodology, Writing – original draft. **Swati Sharma:** Investigation, Writing – review & editing. **Laipubam Gayatri Sharma:** Investigation, Writing – review & editing. **Lalit M. Pandey:** Conceptualization, Formal analysis, Resources, Software, Supervision, Writing – original draft, Writing – review & editing. **Uday Shanker Dixit:** Conceptualization, Formal analysis, Resources, Software, Supervision, Writing – original draft, Writing – review & editing.

Declaration of competing interest

The authors declare that there is no conflict of interest.

Acknowledgement

The authors would like to acknowledge the Central Instrument Facility (CIF), of IIT Guwahati for providing all necessary instrumentation facilities. Recombinant SARS-CoV-2 soluble stabilized spike was obtained through BEI Resources, NIAID, NIH.

References

[1] L.M. Pandey, Surface engineering of personal protective equipments (PPEs) to prevent the contagious infections of SARS-CoV-2, Surf. Eng. 36 (9) (2020) 901–907.
[2] M. Conde-Cid, M. Arias-Estevez, A. Nunez-Delgado, SARS-CoV-2 and other pathogens could be determined in liquid samples from soils, Environ. Pollut. 273 (2021), 116445.
[3] M. Conde-Cid, M. Arias-Estévez, A. Núñez-Delgado, How to study SARS-CoV-2 in soils? Environ. Res. 198 (2021), 110464.
[4] A. Nunez-Delgado, SARS-CoV-2 in soils, Environ. Res. 190 (2020), 110045.
[5] R. Cela-Dablanca, V. Santas-Miguel, D. Fernandez-Calvino, M. Arias-Estevez, M. J. Fernandez-Sanjurjo, E. Alvarez-Rodriguez, A. Nunez-Delgado, SARS-CoV-2 and other main pathogenic microorganisms in the environment: situation in Galicia and Spain, Environ. Res. 197 (2021), 111049.
[6] W. Zeng, G. Liu, H. Ma, D. Zhao, Y. Yang, M. Liu, A. Mohammed, C. Zhao, Y. Yang, J. Xie, C. Ding, X. Ma, J. Weng, Y. Gao, H. He, T. Jin, Biochemical characterization of SARS-CoV-2 nucleocapsid protein, Biochem. Biophys. Res. Commun. 527 (3) (2020) 618–623.
[7] Z. Li, J.D. Hirst, Computed optical spectra of SARS-CoV-2 proteins, Chem. Phys. Lett. 758 (2020), 137935.
[8] S.M. Lokman, M. Rasheduzzaman, A. Salauddin, R. Barua, A.Y. Tanzina, M. H. Rumi, M.I. Hossain, A. Siddiki, A. Mannan, M.M. Hasan, Exploring the genomic and proteomic variations of SARS-CoV-2 spike glycoprotein: a computational biology approach, Infect. Genet. Evol. 84 (2020), 104389.
[9] E.M. Darmady, K.E. Hughes, J.D. Jones, D. Prince, W. Tuke, Sterilization by dry heat, J. Clin. Pathol. 14 (1) (1961) 38–44.
[10] W.B. Hugo, A brief history of heat and chemical preservation and disinfection, J. Appl. Bacteriol. 71 (1) (1991) 9–18.
[11] M. Boudam, M. Moisan, Synergy effect of heat and UV photons on bacterial-spore inactivation in an N2–O2 plasma-afterglow sterilizer, J. Phys. D. Appl. Phys. 43 (29) (2010), 295202.
[12] S. SivaKumar, R. Naveen, D. Dhabliya, B.M. Shankar, B.N. Rajesh, Electronic currency note sterilizer machine, Mater.TodayProc. 37 (2021) 1442–1444.
[13] L. Liao, W. Xiao, M. Zhao, X. Yu, H. Wang, Q. Wang, S. Chu, Y. Cui, Can N95 respirators be reused after disinfection? How many times? ACS Nano 14 (5) (2020) 6348–6356.
[14] L.F. Ludwig-Begall, C. Wielick, L. Dams, H. Nauwynck, P.F. Demeuldre, A. Napp, J. Laperre, E. Haubruge, E. Thiry, The use of germicidal ultraviolet light, vaporized hydrogen peroxide and dry heat to decontaminate face masks and filtering respirators contaminated with a SARS-CoV-2 surrogate virus, J. Hosp. Infect. 106 (3) (2020) 577–584.
[15] N. Mahanta, V. Saxena, L.M. Pandey, P. Batra, U.S. Dixit, Performance study of a sterilization box using a combination of heat and ultraviolet light irradiation for the prevention of COVID-19, Environ. Res. 198 (2021), 111309.
[16] N. Jacobs, K. Chan, V. Leso, A. D'Anna, D. Hollins, I. Iavicoli, A critical review of methods for decontaminating filtering facepiece respirators, Toxicol. Ind. Health 36 (9) (2020) 654–680.

[17] B. Sarada, R. Vijay, R. Johnson, T. Rao, G. Padmanabham, Fight against COVID-19: ARCI's technologies for disinfection, Trans.Indian Natl.Acad.Eng. 5 (2) (2020) 349–354.
[18] C.P. Sabino, A.R. Ball, M.S. Baptista, T. Dai, M.R. Hamblin, M.S. Ribeiro, A. L. Santos, F.P. Sellera, G.P. Tegos, M. Wainwright, Light-based technologies for management of COVID-19 pandemic crisis, J. Photochem. Photobiol. B 212 (2020), 111999.
[19] J.Y. Liang, C.W. Cheng, C.H. Yu, L.Y. Chen, Investigations of blue light-induced reactive oxygen species from flavin mononucleotide on inactivation of E. coli, J. Photochem. Photobiol. B 143 (2015) 82–88.
[20] B. Damit, C. Lee, C.Y. Wu, Flash infrared radiation disinfection of fibrous filters contaminated with bioaerosols, J. Appl. Microbiol. 110 (4) (2011) 1074–1084.
[21] G. Molin, K. Östlund, Dry-heat inactivation ofBacillus subtilis spores by means of infra-red heating, Antonie Van Leeuwenhoek 41 (1) (1975) 329–335.
[22] T.R. Abdussamad, B.A. Rasco, S.S. Sablani, Ultraviolet-C light sanitization of English cucumber (Cucumis sativus) packaged in polyethylene film, J. Food Sci. 81 (6) (2016) E1419–E1430.
[23] G. Yadav, N. Gupta, M. Sood, N. Anjum, A. Chib, Infrared heating and its application in food processing, Pharma Innov.J. 9 (2) (2020) 142–151.
[24] S. Katsura, T. Furuishi, H. Ueda, E. Yonemochi, Cholesteryl-conjugated ribonuclease a exhibits enzyme activity in aqueous solution and resistance to dimethyl sulfoxide, ACS Omega 6 (1) (2021) 533–543.
[25] J. Torrent, S. Marchal, M. Ribo, M. Vilanova, C. Georges, Y. Dupont, R. Lange, Distinct unfolding and refolding pathways of ribonuclease a revealed by heating and cooling temperature jumps, Biophys. J. 94 (10) (2008) 4056–4065.
[26] M. Yujie, Z. Rae, R. Kurt, B. Kelly, Effect of ultraviolet C disinfection treatment on the nanomechanical and topographic properties of N95 respirator filtration microfibers, MRS Adv. 5 (56) (2020) 2863–2872.
[27] P. Zrimsek, J. Kunc, M. Kosec, J. Mrkun, Spectrophotometric application of resazurin reduction assay to evaluate boar semen quality, Int. J. Androl. 27 (1) (2004) 57–62.
[28] M. Zare, M.M. Amin, M. Nikaeen, B. Bina, H. Pourzamani, A. Fatehizadeh, E. Taheri, Resazurin reduction assay, a useful tool for assessment of heavy metal toxicity in acidic conditions, Environ. Monit. Assess. 187 (5) (2015) 276.
[29] P. Costa, A. Gomes, M. Braz, C. Pereira, A. Almeida, Application of the resazurin cell viability assay to monitor Escherichia coli and Salmonella typhimurium inactivation mediated by phages, Antibiotics (Basel) 10 (8) (2021) 974.
[30] M.V. Lancaster R.D. Fields Antibiotic and cytotoxic drug susceptibility assays using resazurin and poising agents Google Patents 1996.
[31] V. Saxena, P. Chandra, L.M. Pandey, Design and characterization of novel Al-doped ZnO nanoassembly as an effective nanoantibiotic, Appl. Nanosci. 8 (8) (2018) 1925–1941.
[32] K. Krishnamurthy, J.C. Tewari, J. Irudayaraj, A. Demirci, Microscopic and spectroscopic evaluation of inactivation of Staphylococcus aureus by pulsed UV light and infrared heating, Food Bioprocess Technol. 3 (1) (2010) 93–104.
[33] C.B. Fowler, D.L. Evers, T.J. O'Leary, J.T. Mason, Antigen retrieval causes protein unfolding: evidence for a linear epitope model of recovered immunoreactivity, J. Histochem. Cytochem. 59 (4) (2011) 366–381.
[34] L.G. Sharma, L.M. Pandey, Shear-induced aggregation of amyloid β (1–40) in a parallel plate geometry, J. Biomol. Struct. Dyn. 39 (17) (2021) 6415–6423.
[35] A. Hasan, V. Saxena, L.M. Pandey, Surface functionalization of Ti6Al4V via self-assembled monolayers for improved protein adsorption and fibroblast adhesion, Langmuir 34 (11) (2018) 3494–3506.
[36] S. Yang, Q. Zhang, H. Yang, H. Shi, A. Dong, L. Wang, S. Yu, Progress in infrared spectroscopy as an efficient tool for predicting protein secondary structure, Int. J. Biol. Macromol. 206 (2022) 175–187.
[37] D. Iannazzo, A. Pistone, I. Ziccarelli, S. Galvagno, Graphene-based materials for application in pharmaceutical nanotechnology, in: Fullerens, Graphenes And Nanotubes, Elsevier, 2018, pp. 297–329.
[38] L. Zhang, D.N. Lu, Z. Liu, How native proteins aggregate in solution: a dynamic Monte Carlo simulation, Biophys. Chem. 133 (1–3) (2008) 71–80.
[39] V. Militello, V. Vetri, M. Leone, Conformational changes involved in thermal aggregation processes of bovine serum albumin, Biophys. Chem. 105 (1) (2003) 133–141.
[40] L.G. Sharma, L.M. Pandey, Thermomechanical process induces unfolding and fibrillation of bovine serum albumin, Food Hydrocoll. 112 (2021), 106294.
[41] Y. Tanaka, Y. Tsunemi, M. Kawashima, H. Nishida, The impact of near-infrared in plastic surgery, Plast.Surg. 2013 (2013) g1–g13.
[42] M.L. Calderon-Miranda, G.V. Barbosa-Canovas, B.G. Swanson, Transmission electron microscopy of Listeria innocua treated by pulsed electric fields and nisin in skimmed milk, Int. J. Food Microbiol. 51 (1) (1999) 31–38.
[43] H. Liu, Y.M. Du, X.H. Wang, L.P. Sun, Chitosan kills bacteria through cell membrane damage, Int. J. Food Microbiol. 95 (2) (2004) 147–155.
[44] H. Liu, I. Elkin, J. Chen, A.M. Klibanov, Why do some immobilized N-alkylated polyethylenimines far surpass others in inactivating influenza viruses? Biomacromolecules 16 (1) (2015) 351–356.
[45] S.L. Rath, K. Kumar, Investigation of the effect of temperature on the structure of SARS-CoV-2 spike protein by molecular dynamics simulations, Front. Mol. Biosci. 7 (2020), 583523.
[46] P. Pecher, U. Arnold, The effect of additional disulfide bonds on the stability and folding of ribonuclease A, Biophys. Chem. 141 (1) (2009) 21–28.
[47] J. Kong, S. Yu, Fourier transform infrared spectroscopic analysis of protein secondary structures, Acta Biochim. Biophys. Sin. Shanghai 39 (8) (2007) 549–559.
[48] H. Singh, R. Jakhar, N. Sehrawat, Designing spike protein (S-Protein) based multi-epitope peptide vaccine against SARS COVID-19 by immunoinformatics, Heliyon 6 (11) (2020), e05528.
[49] S. Kumar, T.S. Thambiraja, K. Karuppanan, G. Subramaniam, Omicron and Delta variant of SARS-CoV-2: a comparative computational study of spike protein, J. Med. Virol. 94 (4) (2022) 1641–1649.
[50] J. Lan, J. Ge, J. Yu, S. Shan, H. Zhou, S. Fan, Q. Zhang, X. Shi, Q. Wang, L. Zhang, X. Wang, Structure of the SARS-CoV-2 spike receptor-binding domain bound to the ACE2 receptor, Nature 581 (7807) (2020) 215–220.
[51] A.B. Ghisaidoobe, S.J. Chung, Intrinsic tryptophan fluorescence in the detection and analysis of proteins: a focus on Förster resonance energy transfer techniques, Int. J. Mol. Sci. 15 (12) (2014) 22518–22538.
[52] J.R. Lakowicz, Principles of Fluorescence Spectroscopy, Springer, New York, NY, 2006.
[53] S.D. Stelea, P. Pancoska, A.S. Benight, T.A. Keiderling, Thermal unfolding of ribonuclease A in phosphate at neutral pH: deviations from the two–state model, Protein Sci. 10 (5) (2001) 970–978.
[54] M. Kowacz, P. Warszynski, Effect of infrared light on protein behavior in contact with solid surfaces, Colloids Surf.A 557 (2018) 94–105.
[55] L.M. Pandey, Physicochemical factors of bioprocessing impact the stability of therapeutic proteins, Biotechnol. Adv. 55 (2022), 107909.
[56] R.E. Hubbard, M.K. Haider, Hydrogen bonds in proteins: role and strength, In: Encyclopedia of Life Sciences (ELS), John Wiley & Sons, Chichester (2010), https://doi.org/10.1002/9780470015902.a0003011.pub2.